



**HAL**  
open science

# Gas-Liquid Flow Characterization and Mass Transfer Study in a Microreactor for Oligomerization Catalyst Testing

Mahmoud Kamaledine, Charles Bonnin, Typhène Michel, Léna Brunet-Errard, Joelle Aubin, Laurent Prat

► **To cite this version:**

Mahmoud Kamaledine, Charles Bonnin, Typhène Michel, Léna Brunet-Errard, Joelle Aubin, et al.. Gas-Liquid Flow Characterization and Mass Transfer Study in a Microreactor for Oligomerization Catalyst Testing. *Chemical Engineering and Processing: Process Intensification*, 2021, 166, pp.108476. 10.1016/j.cep.2021.108476 . hal-03286854

**HAL Id: hal-03286854**

**<https://ifp.hal.science/hal-03286854>**

Submitted on 15 Jul 2021

**HAL** is a multi-disciplinary open access archive for the deposit and dissemination of scientific research documents, whether they are published or not. The documents may come from teaching and research institutions in France or abroad, or from public or private research centers.

L'archive ouverte pluridisciplinaire **HAL**, est destinée au dépôt et à la diffusion de documents scientifiques de niveau recherche, publiés ou non, émanant des établissements d'enseignement et de recherche français ou étrangers, des laboratoires publics ou privés.

**Title: Gas-liquid flow characterization and mass transfer study in a microreactor for oligomerization catalyst testing**

**Author names and affiliations**

Mahmoud Kamaledine<sup>a</sup>

Dr Charles Bonnin<sup>a,\*</sup>

Dr Typhène Michel<sup>b</sup>

Dr Léna Brunet-Errard<sup>c</sup>

Dr Joëlle Aubin<sup>d</sup>

Pr Laurent Prat<sup>d</sup>

<sup>a</sup>IFP Energies Nouvelles, Process Experimentation Division, Rond-point de l'échangeur de Solaize, 69360 Solaize, France.

<sup>b</sup>IFP Energies Nouvelles, Catalysis and Separation Division, Rond-point de l'échangeur de Solaize, BP3, 69360 Solaize, France

<sup>c</sup>IFP Energies Nouvelles, Open Innovation and Incubation Division, 1-4 avenue de Bois-Préau, 92852 Rueil-Malmaison, France

<sup>d</sup>Université de Toulouse, Laboratoire de Génie Chimique, CNRS, 4 allée Emile Monso, 31432 Toulouse, France

Email corresponding author: charles.bonnin@ifpen.fr

**Abstract**

The acceleration of the development of ethylene oligomerization processes by homogeneous catalysis requires a complete characterization of the catalytic system. This work proposes to use segmented gas-liquid flow in microchannels to achieve high experimental throughput for catalyst testing.

Gas-liquid flow was studied in order to validate the microreactor setup. Results showed that bubble and slug lengths vary linearly with the superficial velocities ratio following the Garstecki et al model [21]. The impact of lateral feed in Taylor flow was explored to mimic the catalyst feed in an oligomerization test. The experiments showed that the volume of the liquid slugs increased proportionally to the additional flow rate, thereby suggesting that the majority of the liquid in the lateral feed is ultimately retained in the liquid slug.

A study of mass transfer showed that the volumetric mass transfer coefficient is between 0.27 and 0.55  $s^{-1}$ . These values lead to a Hatta number  $< 0.5$ , thus confirming the possibility of conducting the ethylene oligomerization reaction in the chemical kinetic regime.

Finally, an ethylene oligomerization test performed in the microreactor showed that the continuous microreactor system can be used for catalyst screening purpose.

**Keywords:** Homogeneous catalysis, Mass transfer, Microreactor, Oligomerization, Taylor flow

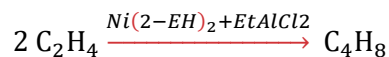
## 1 Introduction

### 1.1 Study context and objectives

The oligomerization of ethylene is a reaction that produces linear alpha-olefins that are mainly used as co-monomers for the production of polyethylene, which is a raw material that has a growing demand in the world market. In order to meet this need, oligomerization processes have been the subject of intensive research in the last decades [1–3]. Processes and catalytic systems for this reaction are continuously being developed due to the on-going change in the market of linear alpha olefins. Today, the demand for short-chain  $C_4$  to  $C_8$  linear alpha olefins is growing faster than that for linear alpha olefins in the  $C_8^+$  range. Hence, there is a need to identify high performance catalysts and develop selective processes in order to produce short-chain linear alpha olefins directly, or even one main alpha olefin like 1-butene, 1-hexene or 1-octene. In addition, this oligomerization reaction is of environmental interest as it is essential for the development of new systems for the production of linear olefins from ethylene produced from renewable resources, such as bio-ethanol.

The oligomerization of ethylene with a homogeneous catalytic system is a two-phase exothermic reaction (about 25-30  $kcal.mol^{-1}$  of transformed  $C_2H_4$ ) that takes place under moderate conditions of pressure (10-30 bar) and temperature (30-50°C). In this reaction, gaseous ethylene is converted into linear alpha-olefins in the presence of an organometallic catalyst. Both the ethylene and the catalytic system are dissolved in an organic liquid phase where the reaction takes place.

The catalytic system chosen to carry out the dimerization of ethylene to butene in this study is composed of a nickel-based catalytic precursor (nickel (II) 2-ethylhexanoate), activated *in-situ* by an aluminum-based activator (ethylaluminium dichloride). The principle reaction is the following:



In the liquid phase, the catalytic system is mixed with an organic solvent, which is cyclohexane. Due to the sensitivity of the catalytic system, this reaction must be performed in the absence of any traces of humidity. The main product is 1-Butene, but during reaction other C<sub>4</sub> isomers and heavier olefins are also produced.

Fed-batch stirred-tank reactors are typically used for the identification and development of the catalytic system required for this type of reactions. However, it is well known that temperature control is poor in fed-batch stirred-tank reactors, and particularly when there is a fast rise in temperature at the beginning of the reaction, which is the case for oligomerization reactions. Temperature is better controlled in continuous processes, however, the testing time for a catalytic system using a continuous stirred-tank reactor is long. It takes approximately one week to perform the tests on one system due to the time required to reach the desired catalyst concentration at the beginning of the test, the time to adjust the operating parameters, and to shut down the unit at the end of a test. However, microreactors with continuous flow operation offer the possibility to perform tests on catalytic systems much more quickly. Indeed, microreactors allow good heat control, as well as intensified kinetic data acquisition since it is possible to quickly modify the tested catalytic system or the operating conditions, as well as start-up and shut-down of the reactor. In addition, the use of microreactors enables smaller amounts of reactants to be consumed since the testing volume is drastically smaller than that of stirred tanks – several milliliters in microreactors compared with several hundreds of milliliters in stirred-tank reactors.

The interest of using microreactors as a testing tool for kinetic studies and catalyst screening of two-phase reactions has been demonstrated in numerous studies [e.g. 4–8]. The comparison between the tests performed in a microreactor with those performed in a batch reactor have shown that the former provides better control of mass transfer [4,9,10] and allows a significant increase in the number of tests

carried out over a given period [7]. Indeed, in the case of two-phase flows in microchannels, segmented flow or Taylor flow – whereby the dispersed phase forms very regular bubbles or droplets – provides high interfacial area for mass transfer and excellent mixing of small amounts of reactants [11].

In this study, a microreactor testing unit is developed for the ethylene oligomerization reaction. In order to develop this unit, it is necessary to characterize the reactor performance in terms of hydrodynamics and mass transfer for several reasons:

- The microreactor is to be operated with Taylor flow, also known as slug flow, which is characterized by the presence of elongated gas bubbles with lengths equal to or greater than the hydraulic diameter of the channel, separated from each other by liquid slugs and from the channel wall by a thin liquid film [11]. This flow regime is recognized to be the most advantageous two-phase flow regime for a reaction because of the high interfacial area between phases, as well as the recirculation flow in the liquid slug that promotes mass transfer and allows good mixing of the catalyst feed in the liquid phase. It is therefore important to maintain the Taylor flow regime during a reaction and to avoid the complete consumption/dissolution of the gas bubbles. It is therefore important to control two parameters: the reaction rate and the bubble length. The reaction rate depends on operating conditions and can be estimated using kinetic models obtained with stirred tank reactors. Once the reaction rate is known, it is possible to estimate the minimum bubble length to maintain Taylor flow. To control this bubble length, an equation for the estimation of the bubble length in function of the gas and liquid flow rates is required;
- Using microreactor technology for catalyst development for ethylene oligomerization presents another particular challenge, which is the need to inject several liquid feeds into the Taylor flow. Indeed, the catalytic system is composed of two liquid components, which should not be mixed in the absence of ethylene to achieve good catalytic performance and to avoid the potential deactivation of the catalytic system. Gaseous ethylene is therefore firstly dispersed into the liquid solvent before the liquid catalytic components are injected into the flow. Thus, it is

important to verify that all liquid slugs receive the same amount of catalyst in order to have a homogenous catalyst concentration along the microreactor;

- As the oligomerization reaction can take place under different pressures and temperatures, the determination of the impact of these two parameters on bubble volume can guide the choice of the operating conditions;
- For kinetic studies, it is also important to determine the operating range for which the reaction will not be limited by mass transfer. In addition to the nature of the studied binary, the mass transfer coefficient is influenced by the geometry and size of the channel [12], as well as by the gas-liquid flow rate [13]. Thus, the rate of mass transfer can vary strongly with operating conditions and from one microreactor system to another, as shown in the Tab. 1. Therefore, before starting catalytic tests, a mass transfer study is necessary in order to verify that the reaction is not limited by mass transfer in the range of operating conditions.

**Table 1.** Order of magnitude of the global mass transfer coefficient for selected experimental studies of mass transfer in milli- and microchannels.

Authors	Phases (gas-liquid)	Channel hydraulic diameter [mm]	Flow velocity [m.s <sup>-1</sup> ]	$K_L a$ range [s <sup>-1</sup> ]
Irandoost et al., 1992 [12]	Air - water Air - Ethanol Air - Ethylene glycol	2.2	0.092 - 0.56	0.01 - 0.3
Bercic and Pintar, 1997 [13]	Methane - Water	1.5; 2.5; 3.1	0.01 - 0.5	0.01 - 0.3
Vandu et al., 2005 [14]	Air - Water	1; 2; 3	0.04 - 0.6	0.04 - 0.8
Yue et al., 2007 [15]	CO <sub>2</sub> - Water	0.667	1 - 14	1 - 18
Yue et al., 2009 [16]	Air - Water	0.2; 0.4	0.2 - 2.2	3-9
Kuhn and Jensen, 2012 [17]	CO <sub>2</sub> - Alkine solution	0.4	~0.026	0.05 - 1.0
Dietrich et al., 2013 [18]	Air - Water	2	0.01-0.51	0.1 - 0.5
Yao et al., 2014 [19]	CO <sub>2</sub> - Ethanol/water	0.4	0.1-0.5	1 - 6
Deleau et al., 2020 [20]	CO <sub>2</sub> - Water	0.3	0.24 - 0.72	0.002 - 0.05

The objective of this work is therefore to develop a new experimental unit for the transposition of homogeneous catalytic tests for ethylene oligomerization reactions, which are typically performed in a batch reactor, to a continuous flow microreactor. The microreactor in the new set up is to be operated in the Taylor flow regime and it is therefore necessary to characterize this flow in terms of gas-liquid

hydrodynamics and mass transfer, as well as reaction performance in order to answer the four previously mentioned points. To do this, a series of experiments are firstly performed with N<sub>2</sub>-cyclohexane binary in order to characterize the gas and liquid lengths as a function of the flow rates of the two phases, as well as the impact of the pressure and temperature on the bubble volume without mass transfer. Furthermore, a lateral liquid feed is introduced in order to evaluate the stability of the Taylor flow when liquid catalyst is added and to verify that the catalyst is equally distributed between liquid slugs. Secondly, mass transfer is evaluated for a non-reactive ethylene-cyclohexane flow. A visual method that consists of tracking the change in bubble size along the microchannel with a high-speed camera is used to determine the mass transfer coefficient. Finally, the ethylene oligomerization reaction is performed in the new microreactor experimental unit, in order to validate the proof-of-concept.

## 1.2 hydrodynamics and bubble length of Taylor flow

Taylor flow has been the subject of numerous studies that have sought to characterize the flow regime and to understand the influence of operating conditions (e.g. fluids superficial velocities, fluids properties, pressure) and geometrical parameters (e.g. channel diameter, cross-sectional geometry). A well-known model for estimating bubble size in Taylor flow is that proposed by Garstecki et al [21], which describes bubble formation in a T-junction (with rectangular cross-section) in the squeezing regime where the interfacial forces dominate shear stresses (capillary number  $Ca < 10^{-2}$ ) and inertial effects are negligible (Reynolds number  $Re < 1$ ). The model considers the generation of two-phase flow when the continuous phase is injected in the main channel of width  $w$  and the dispersed phase is injected perpendicular to the main flow via a side channel of width  $w_{in}$  and describes the mechanism for bubble generation in two steps. In the first stage, the dispersed phase fills and blocks the main channel and in the second stage, the bubble keeps growing until it is pinched off by the continuous phase. Thus, Taylor bubble generation can be described by a characteristic time for bubble generation  $t_{gen}$ , which is the sum of the time required for the gas phase to block the main channel,  $t_{fill}$ , and the time for the bubble to be pinched off by the continuous phase,  $t_{squeeze}$ .

Garstecki et al. [21] estimated that the initial bubble length at the end of the first stage is approximately equal to the width of the main channel. Following the blockage of the main channel, the continuous phase flow will then squeeze the bubble neck of a characteristic width  $d$ . During the filling stage, the bubble grows with a speed equal to the superficial velocity of the dispersed phase, while the characteristic time for squeezing depends on the superficial velocity of the continuous phase. Following this, the final bubble length can be expressed by the equation (1):

$$L_B \approx w + d \frac{U_G}{U_L} \quad (1)$$

where  $U_G$  and  $U_L$  are the superficial velocities of the dispersed phase and the continuous phase, respectively,  $w$  the width of the main channel and  $d$  the characteristic width of the bubble neck.

The dimensionless equation is:

$$\frac{L_B}{w} = 1 + \alpha \frac{U_G}{U_L} \quad (2)$$

with  $\alpha = d/w$ . Taking into consideration that part of the continuous phase flow will bypass the bubble during the squeezing stage and will not contribute to the decrease in the bubble neck, Garstecki et al. [21] considered that it is reasonable to treat  $\alpha$  as a fitting parameter. Indeed, Van Steijn et al. [22] showed that the bubble does not block the entire cross section of the main channel during the formation and that at least 10% of the continuous phase flow rate  $Q_L$  leaks through the gaps during the bubble generation. van Steijn et al [22] proposed equation (3) with coefficient  $\alpha_1$  for the first term, instead of 1, that takes into account the deviation of the bubble length at the end of the filling stage from the hypothetical value of  $w$ .

$$\frac{L_B}{w_{in}} = \alpha_1 + \alpha_2 \frac{Q_G}{Q_L} \quad (3)$$

where  $\alpha_1$  and  $\alpha_2$  are constants that depend on the geometry of the T-junction. van Steijn et al [22] showed with microPIV measurements that the characteristic width of the rising bubble neck  $d$  is approximately equal to the width of the dispersed phase inlet,  $w_{in}$ . When  $L_B$  is normalized with  $w_{in}$ , as

in equation (3),  $\alpha_1$  tends towards  $w/w_{in}$  in the case of flat ended bubbles with no surrounding liquid film and  $\alpha_2$  tends towards 1 when there is no liquid leakage.

### 1.3 Mass transfer in microreactors

In order to quantify gas-liquid mass transfer in microreactors, many methods and techniques have been applied in the literature. These methods can be divided into two main categories: global measurements and online measurements.

Global measurement methods consist of determining the quantity of gas absorbed in the liquid phase by comparing the phase composition at two positions, typically the inlet and outlet. The concentration of the gas in the liquid phase can be measured continuously [14], using an analyzer placed at the reactor outlet, or discontinuously by delocalized analyses [15]. In the second case, particular attention must be paid to sampling in order to ensure that the gas remains dissolved in the liquid phase. The main disadvantage of these methods is the time delay related to the need to accumulate a certain sample volume at the output of the system, especially at low flow rates. Furthermore, such methods provide  $K_L a$  values that are an average over the reactor length.

Online methods usually employ optical methods based on image processing of photos taken at different points in the channel using a high-speed camera. Mass transfer can be observed by several techniques, which may be a simple analysis of the bubble size evolution [19,23–25], or a change in color [18] or fluorescence [17]. The main advantage of the online methods is that they allow mass transfer to be monitored throughout the reactor, and thus giving access to local values of the mass transfer coefficient. Another recently employed online method is Raman spectroscopy, which can be used to measure the fraction of gas dissolved in the liquid phase at different points along the capillary [20]. The mass transfer coefficient may be then deduced from the concentration values, which vary along the length of the microchannel.

Mass transfer in Taylor flow has been discussed significantly in the literature and various models and correlations have been proposed [11,26,27] to estimate the mass transfer coefficient for operating parameters. It has largely been shown that gas-liquid mass transfer in Taylor flow has two contributions:

the transfer of gas molecules from the bubble into the liquid slug through the caps of the bubble, and the transfer of gas from the bubble to the liquid film surrounding the bubble body. Van Baten and Krishna [28] were the first to model mass transfer in Taylor flow in small channels. Their model uses the "Higbie penetration" theory and takes into account the contribution of both the bubble caps and body in order to estimate the mass transfer coefficient. Vandu et al. [14] applied this model to their experimental mass transfer results obtained for an air-water flow in capillaries of 1, 2 and 3 mm diameters and found that the model of van Baten and Krishna [28] described their experimental  $K_L a$  values reasonably well. Vandu et al. [14] then simplified this model by identifying the conditions for which the transfer into the liquid film is dominant and by adding a fitting parameter to the model. Pohorecki [36] also proposed a criterion that should be met in order to avoid saturation of the liquid film surrounding the bubble:

$$\frac{L_B D_{iff}}{U_{TP} \delta^2} \ll 1 \quad (4)$$

With  $D_{iff}$  the gas diffusion rate,  $U_{TP}$  the two phases superficial velocity and  $\delta$  the liquid film thickness.

## 2 Material and methods

### 2.1 Experimental set-up

Fig. 1 shows a schematic representation of the experimental set-up for hydrodynamic tests. Taylor flow is generated in a stainless steel T-junction with circular cross-section and  $D_T=0.5$  mm internal diameter. The liquid phase is injected in the main channel of the T-junction and the gas phase is injected from the side. The gas-liquid dispersion flows into a fused silica capillary (internal diameter  $D_{ch}=0.53$  mm, length 8 cm), which is followed by another stainless steel T-junction with circular cross-section and 0.5 mm internal diameter. The second T-junction is used to feed an additional liquid to the gas-liquid flow in order to mimic the injection of the liquid catalyst in the oligomerization reaction. The gas-liquid dispersion then flows into the main channel, which is a fused silica capillary with an internal diameter of 0.53 mm and 1.5 m in length.

In order to control the temperature in the microfluidic system, the ensemble of T-junctions and capillary tubes are immersed in a heated water bath that circulates in an etched Poly(methyl methacrylate) (PMMA) plate.

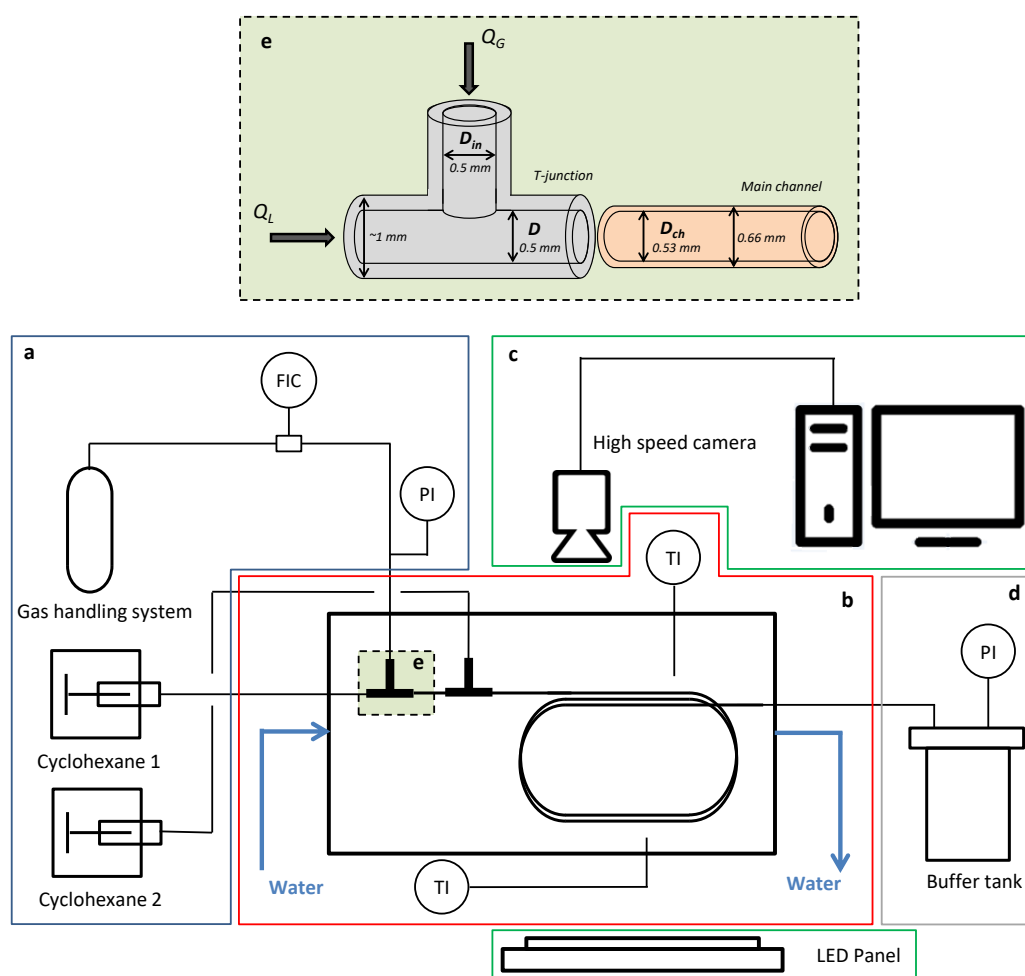


**Figure 1.** Experimental set-up for hydrodynamic tests, a) injection system: gas source and liquid pumps b) microreactor placed in a PMMA plate with water circulation c) image acquisition system d) pressure regulation system e) dimensions of the T-junction and the main channel

Each liquid phase is injected using a high-pressure syringe pump, which is equipped with an 8 mL high-pressure stainless steel syringe (Harvard Apparatus). For the gas phase injection, a different flow controller is used depending on the gas type. A thermal mass flow controller and meter (Brooks 5850E) with a range of  $0\text{-}500 \text{ NmL}\cdot\text{h}^{-1}$  is used to control the nitrogen flow rate. The ethylene flow rate was controlled with “mini CORI-FLOW” controller from Bronkhorst with a range of  $0\text{-}5 \text{ g}\cdot\text{h}^{-1}$  since it provided better stability in the delivered flow rate than the thermal mass flow controller. Indeed, the variation of the heat capacity  $C_p$  of ethylene close to the supercritical temperature and pressure ( $T_c = 9.2^\circ\text{C}$ ,  $P_c = 50.4$

bar) does not allow an accurate measurement of the flow rate with the thermal mass flow controller.

The Bronkhorst controller is based on the Coriolis effect and is not affected by this variation in thermal capacity  $C_p$ .

Both gas and liquid phases are collected in a 300 mL buffer tank at the outlet of the microchannel. The buffer tank is filled with nitrogen at the operating pressure (10-27 Barg). Since the flow rate is very low (370 NmL.h<sup>-1</sup> max), the pressure in the vessel (and therefore in the system) is almost constant during an experiment. For a maximum gas flow rate of 370 NmL.h<sup>-1</sup> and at 50°C, the pressure increase is about 0.022 bar.min<sup>-1</sup>. Therefore, for an average data acquisition time of 1 minute, the pressure rise will be negligible and is lower than the precision of the pressure sensors in the system (0.1 bar).

The experimental set up was slightly modified for the oligomerization reaction experiments as shown in Fig. 2. The second T-junction was replaced by a cross junction in order to inject both components (precursor and activator) of the catalytic system. At the outlet of the microreactor, a stainless steel T-junction was added in order to inject a quenching agent to stop the reaction. In addition, the pressure regulation is insured by back pressure controller rather than the buffer tank. At the outlet of the pressure controller, the effluent is vaporized at 140°C and analyzed on-line by gas chromatography (GC). The GC analysis lasts 45 minutes and enables the concentrations of ethylene, 1-butene, cis-2-butene, trans-2-butene, cyclohexane, C<sub>6</sub> olefins and C<sub>8</sub> olefins to be measured. Since cyclohexane is used as a solvent, it is not consumed during the reaction and is therefore used as internal reference to measure the volumetric flow rate at the reactor outlet.

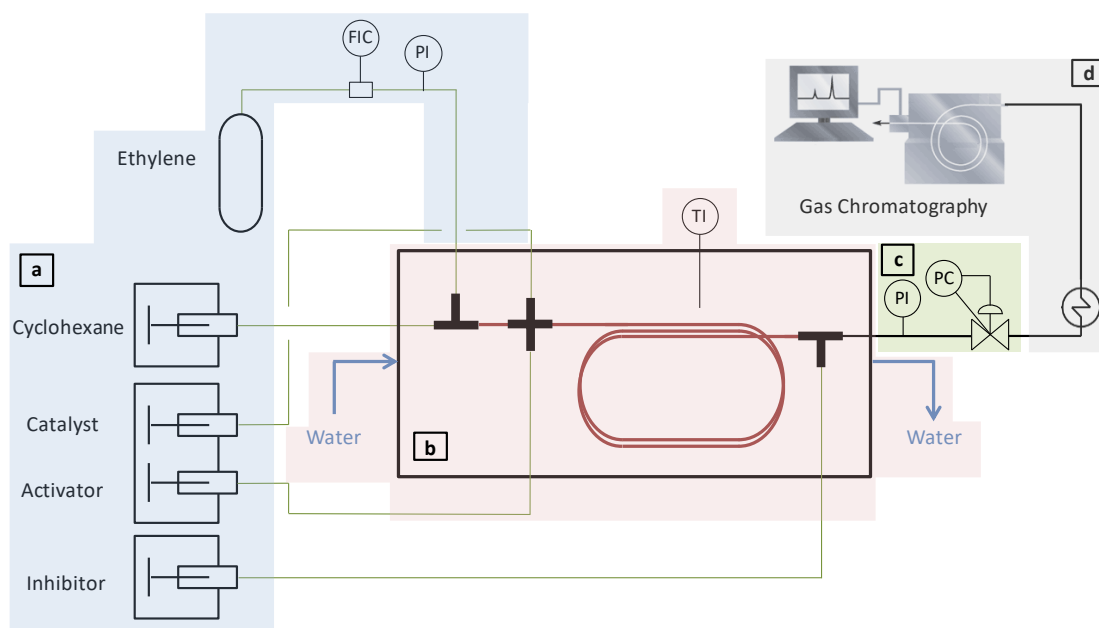


**Figure 2.** Experimental set-up for catalytic tests, a) injection system: gas source and 4 syringe pumps for liquid injections b) reaction zone: microreactor with T-junctions and a cross junction placed in a PMMA plate with water circulation c) pressure regulation system d) online analysis by gas chromatography (GC)

## 2.2 Fluids and operating conditions

### 2.2.1 Hydrodynamic experiments

Before studying non-reactive ethylene-cyclohexane flow for mass transfer, a series of hydrodynamic experiments were performed with  $N_2$  and cyclohexane. Nitrogen was chosen for this study as it has very low solubility in cyclohexane ( $\sim 3.4 \text{ NmL of } N_2 \text{ in } 1 \text{ mL of cyclohexane at } P=20 \text{ bar and } T=25^\circ\text{C}$ ) [37] and thus allows the flow stability and the bubble length to be evaluated. Ethylene-cyclohexane experiments without a catalyst were then conducted in order to evaluate the mass transfer of ethylene into the gas phase without reaction.

The hydrodynamics and mass transfer measurements were conducted at three pressures (10, 20 and 27 barg) and temperatures (30, 40 and  $50^\circ\text{C}$ ), in order to cover the operating conditions in which the reaction of interest can take place. Tab. 2 and Tab. 3 present the principle physical properties (density, liquid viscosity and liquid surface tension) of the different fluids used at the various conditions of pressure and temperature.

**Table 2.** Nitrogen and ethylene density  $\rho$  ( $\text{kg}\cdot\text{m}^{-3}$ ) at different pressure and temperature.

	40°C			20 barg		
	10 barg	20 barg	27 barg	30°C	40°C	50°C
Nitrogen	11.8	22.6	30.2	23.4	22.6	21.9
Ethylene	12.5	25.4	35.4	26.6	25.4	24.3

**Table 3.** Physical properties of cyclohexane at different temperatures.

	Density $\rho$ [kg.m <sup>-3</sup> ]	Dynamic Viscosity $\mu$ [mPa.s]	Liquid surface tension $\sigma_L$ [N.m <sup>-1</sup> ] [38]
30°C	771	0.83	0.0241
40°C	761	0.71	0.0229
50°C	752	0.61	0.0217

The range of flow rates used for all experiments is  $50 < Q_G < 370 \text{ NmL.h}^{-1}$  for the gas phase and  $0.5 < Q_L < 4 \text{ mL.h}^{-1}$  for the total liquid phase at the outlet of the microchannel. These flow rates correspond to the following ranges of superficial velocities, and two-phase Reynolds and capillary numbers:  $0.63 \cdot 10^{-3} < U_L < 3.8 \cdot 10^{-3} \text{ m.s}^{-1}$ ,  $3.4 \cdot 10^{-3} < U_G < 30 \cdot 10^{-3} \text{ m.s}^{-1}$ ,  $0.01 < Re_{TP} < 0.14$  and  $10^{-4} < Ca_{TP} < 10^{-3}$ . Two flow rates were tested ( $0.1 \text{ mL.h}^{-1}$  and  $0.2 \text{ mL.h}^{-1}$ ) for the second liquid injection that was used to mimic the catalyst injection.

Ethylene-cyclohexane is a mixture that can be characterized by either a single-phase liquid or gas, or by a two-phase vapor-liquid system that is in thermodynamic equilibrium, known as vapor-liquid equilibrium (VLE). The boundaries of the single phase liquid, the VLE and the single phase vapor regions depend on pressure, temperature and mixture composition. In this study, the experimental VLE data for ethylene-cyclohexane mixture were compared with those obtained using the Peng-Robinson predictive model (PPR78). This thermodynamic model has been chosen because it is able to correctly represent the fluid phase behavior of fluids containing alkanes, alkenes, aromatic compounds, cycloalkanes, permanent gases ( $\text{CO}_2$ ,  $\text{N}_2$ ,  $\text{H}_2\text{S}$ ,  $\text{H}_2$ ), mercaptans and water [29].

Fig. 3 shows the phase diagram for the cyclohexane-ethylene mixture plotted with the Peng Robinson predictive model. The diagram shows that for the range of operating conditions, two-phase flow is expected for almost all conditions. Indeed, for certain operating conditions (denoted by the green

symbols), the gas phase is completely dissolved in the liquid phase at equilibrium. These conditions are out of the interest of this study since they do not provide Taylor flow.

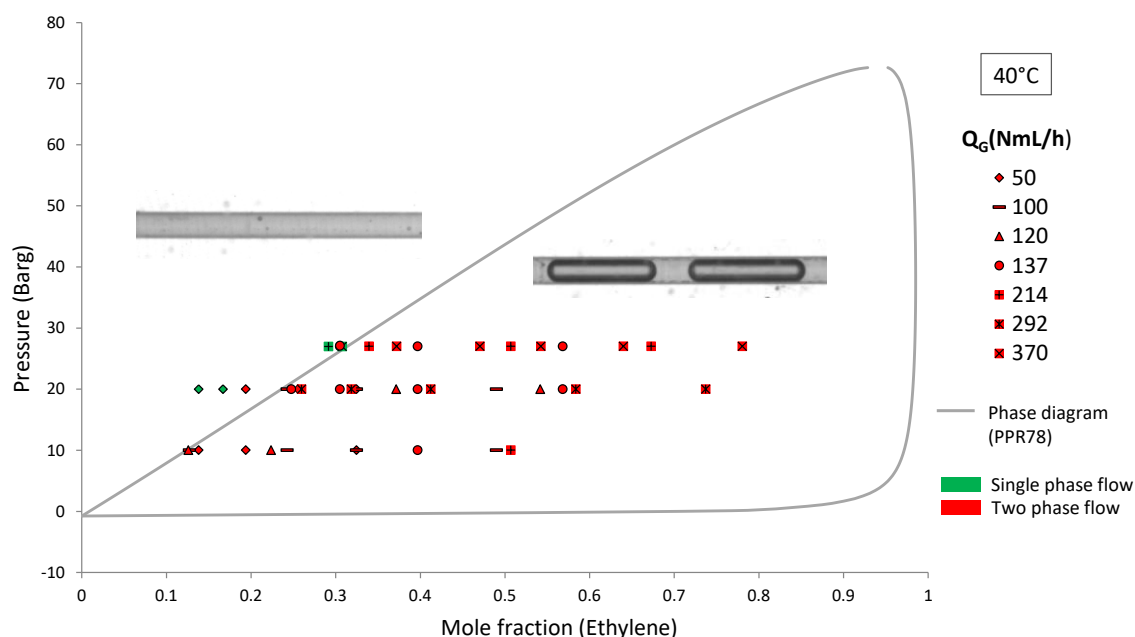


**Figure 3.** The distribution of experimental points on the phase diagram for the cyclohexane-ethylene mixture.

### 2.2.2 Oligomerization reaction

For the oligomerization reaction tests, the operating conditions were chosen based on the results of the hydrodynamic study. A total liquid flow rate of  $1.29 \text{ mL}\cdot\text{h}^{-1}$  with a catalyst concentration of  $31.4 \text{ ppm}$  at the inlet of the reactor and an ethylene flow rate of  $286 \text{ NmL}\cdot\text{h}^{-1}$  were chosen for the catalytic test.

Both precursor and activator solutions were prepared using cyclohexane as a solvent. The prepared precursor solution concentration is  $3 \text{ mmol}\cdot\text{L}^{-1}$  and the activator solution concentration is  $90 \text{ mmol}\cdot\text{L}^{-1}$ . The precursor and activator flow rates are adjusted to maintain an  $[\text{activator}]/[\text{precursor}]$  concentration ratio between 15 and 20 which is known to give optimum catalytic activity in stirred tank reactor tests. At the reactor outlet, the flow rate of the inhibitor solution is set to ensure a molar ratio of inhibitor to activator between 3 and 5.

### 2.3 Image acquisition and measurements

The hydrodynamics and mass transfer in the non-reactive system are evaluated by high-speed imaging and analysis. A LED panel of 30 cm × 20 cm is placed under the PMMA plate in order to ensure lighting for observation and image acquisition of the two-phase flow in the microchannel. A digital camera (EoSens CL MC 1362) with a full resolution of 1280 × 1024 pixels and acquisition rate of 500 frames per second was used to image the flow.

Images analysis is carried out with Fiji software (imageJ) with which a processing procedure has been implemented in order to extract the position and the length of each bubble. Firstly, a mean filter is applied to reduce noise. A threshold module is then applied to the image to isolate the gas-liquid interface (Fig. 4) and finally a plugin to detect shapes ("Analyze particles") is used. The latter returns information such as the geometric center, length, height and surface of each identified shape. This processing procedure is applied to each image. The conversion of a pixel into metric units is carried out with a ruler that appears at the bottom of the images (Fig. 4) and it is adjusted for each image sequence. The bubble length and position data are used to calculate the slug length, which is the distance between two bubbles, as indicated in Fig. 4. For each operating condition, the mean bubble length  $L_B$  and the mean slug length  $L_S$  are calculated using a minimum of 100 bubbles, which was found to be statistically representative. The relative standard deviation (or coefficient of variation) for the majority of the average values is less than 10% for the bubble length and less than 6% for the slug length. The precision of the acquisition method is estimated at  $\pm 4$  pixels. Therefore, only experiments where the decrease in bubble length was greater than 10 pixels were considered for the mass transfer study and the calculation of  $K_L a$ . The velocity of each bubble  $U_B$  was determined from the displacement of the bubble between two image frames.

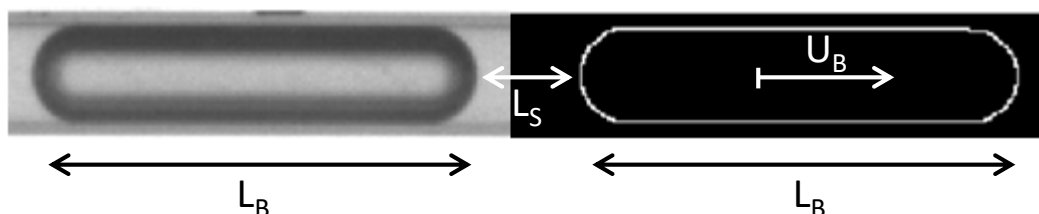


**Figure 4.** A raw photo (left) and a processed photo (right) of a bubble, with the representation of the bubble length, slug length and bubble velocity.

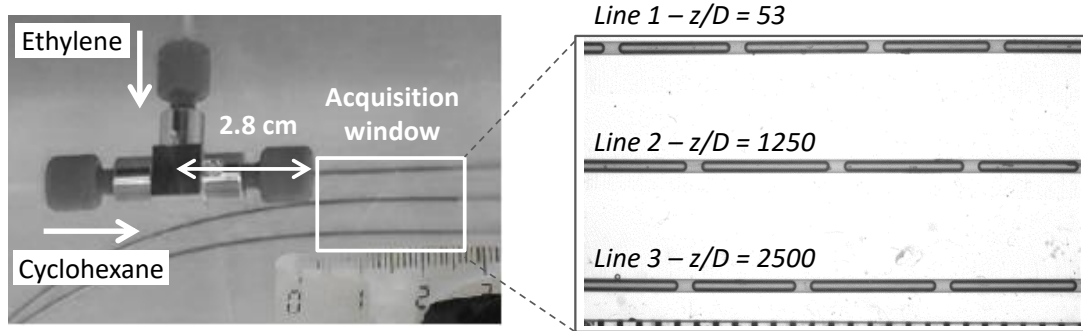


**Figure 5.** Generation T-junction and the acquisition window.

For each test, the volumes of bubbles and slugs were calculated by considering bubbles with a cylindrical body with a diameter equivalent to the inner diameter of the microchannel and a hemispherical head and tail. The former is justified by the fact that the liquid film is considered to be extremely thin for all operating conditions in this study. Indeed, for low capillary numbers ( $<0.01$ ), Bretherton [1] estimated the thickness of the liquid film between the bubble and the wall by the following equation:

$$\frac{\delta}{R} = 1.34 Ca_B^{2/3} \quad (5)$$

where  $\delta$  is the liquid film thickness,  $R$  is the channel radius and  $Ca_B = (\mu_L U_B)/\sigma_L$  is the capillary number based on bubble velocity. In this study,  $Ca_B$  varies between  $10^{-4}$  and  $6 \cdot 10^{-4}$  and using Bretherton's equation (5), the thickness of the liquid film is estimated to be between 0.8 and 2.5  $\mu\text{m}$ , which represents only 0.3 to 1% of the channel radius and 0.6 to 2% of the channel cross-sectional area. Applying equation (4) for the liquid film saturation, values in the order of  $10^3$  are obtained for the Pohorecki's criterion what shows that in the selected conditions, the liquid film will be quickly saturated with ethylene and mass transfer will take place almost exclusively through the bubble caps.

At low capillary numbers ( $<0.01$ ), the head and tail of the bubble are symmetrical and have a hemispherical shape (Fig. 4). Thus, for negligible liquid film, the volume of a bubble  $V_B$  in a channel with

internal diameter  $D$  can be expressed as the sum of the volume of a cylinder with length  $(L_B - D)$  and the volume of two hemispheres of diameter  $D$ :

$$V_B = \frac{\pi D^2}{4} (L_B - D) + \frac{\pi D^3}{6} \quad (6)$$

The bubble surface area can be expressed as the sum of the area of a cylinder with length  $(L_B - D)$  and the area of two hemispheres of diameter  $D$ :

$$A_B = \pi D (L_B - D) + \pi D^2 \quad (7)$$

The slug volume  $V_S$  is then described as difference of the volume of a cylinder with length  $(L_B + L_S)$  and the bubble volume  $V_B$ :

$$V_S = \frac{\pi D^2}{4} (L_B + L_S) - V_B \quad (8)$$

## 2.4 Determination of mass transfer coefficients

For every operating condition, the bubble length was tracked from three different positions in the capillary tube ( $z/D=53$ ,  $z/D=1250$  and  $z/D=2500$ , where  $z$  is the axial position in the channel with  $z=0$  at the center of the T-junction) and over a distance of 2.6 cm, as shown in Fig. 5. Between  $z/D=0$  and  $z/D=53$ , the bubble train cannot be seen because it is in the T-junction. At each position, the length of each bubble is tracked and the mean bubble volume along the length of 2.6 cm is calculated.

In order to quantify mass transfer, the mass transfer coefficient is calculated using the expression given in equation (9) [15,17,23].

$$\frac{d(U_L C_L(z))}{dz} = K_L a (C_L^{eq} - C_L(z)) \quad (9)$$

Where  $C_L$  is the ethylene concentration in the liquid phase,  $C_L^{eq}$  is the ethylene concentration in the liquid phase at thermodynamic equilibrium and  $K_L a$  is the volumetric mass transfer coefficient.

Considering a constant volumetric mass transfer coefficient  $K_L a$  and a constant superficial velocity of the liquid phase, integration of equation (9) between an initial position  $z_i$  and a position  $z$  gives:

$$-\ln \left( \frac{C_L^{eq} - C_L(z)}{C_L^{eq} - C_L^i} \right) = \frac{K_L a}{U_L} (z - z_i) \quad (10)$$

Where  $C_L^i$  is the concentration of ethylene in the liquid phase at position  $z_i$ .

In this study, the concentration terms are replaced by the bubble volume that is calculated from the bubble length measured along the capillary tube. To do so, a unit cell model, which corresponds to the ensemble of one gas bubble and one liquid slug, was considered. This model takes several hypotheses into consideration: there is no mass transfer between two consecutive unit cells; the gas and liquid are in equilibrium at the interface; the gas and liquid phases are well mixed; mass transfer only occurs from the gas to the liquid phase; pressure drop is negligible; liquid volume is constant.

Following these hypotheses, it can also be assumed that the composition of the gas phase does not change as no transfer from the liquid phase to the gas phase will occur. Thus, the molar volume of the gas phase  $v_G$  remains constant. The molar concentration of ethylene in the liquid phase at position  $z$  is related to the variation of bubble volume by the following equation:

$$C_L(z) = \frac{1}{v_G} \left( V_B^0 - V_B(z) \right) \frac{1}{V_S} \quad (11)$$

Where  $V_S$  is the volume of the liquid slug.

Equation (10) can then be written in terms of the bubble volume as follows:

$$-\ln \left( \frac{V_B(z) - V_B^{eq}}{V_B^i - V_B^{eq}} \right) = \frac{K_L a}{U_L} (z - z_i) \quad (12)$$

Where  $V_B(z)$  is the gas bubble volume at position  $z$  and  $V_B^i$  and  $V_B^{eq}$  are the gas bubble volumes at positions  $z_i$  and at the thermodynamic equilibrium, respectively.

### 3 Results and discussions

#### 3.1 Hydrodynamics

##### 3.1.1 Bubble and slug lengths

Fig. 6 shows the variation in bubble length as a function of the superficial velocity ratio of the two phases. The bubble lengths considered in this figure are the lengths in the T-junction where the flow generation occurs. Since the diameter of the T-junction is slightly different than the diameter of the

main channel where the bubble length where measured (as shown in Fig. 1), a correction was applied to the measured bubble lengths.

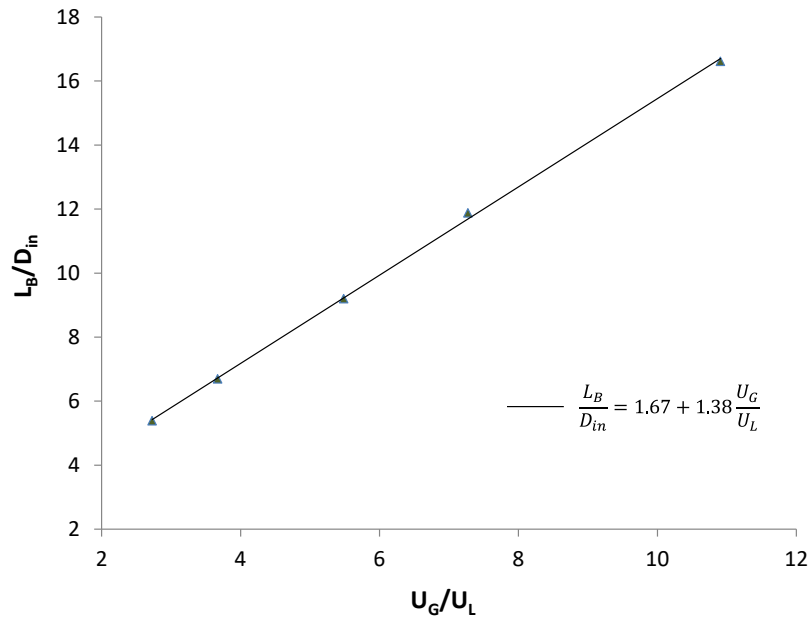


**Figure 6.** Variation of normalized bubble length as a function of superficial velocity ratio ( $N_2$ -cyclohexane,  $T=40^\circ\text{C}$ ,  $P=20$  barg,  $3.4 < U_G < 13.7$  mm.s $^{-1}$ ,  $1.3 < U_L < 1.9$  mm.s $^{-1}$ )

The bubble length increases linearly with the superficial velocity ratio following the model by Garstecki et al. [21]. Considering Equation (3), the coefficients obtained for these bubble lengths are  $\alpha_1 = 1.67$  and  $\alpha_2 = 1.38$ , which are very close to those found by Van Steijn et al [22] who obtained  $\alpha_1 = \alpha_2 = 1.5$  in a square cross-sectional channel.

Van Steijn et al [22] also showed for an air-ethanol flow in a square cross-sectional channel that after the filling phase, the main channel is not completely blocked by the gas phase and therefore results in liquid leakage during the bubble squeezing phase. The leakage flow results in a longer squeezing time and thus a longer gas bubble, which is taken into account by the coefficient  $\alpha_2 > 1$ . Leclerc et al [30] also worked on a rectangular cross section and tested different T-junction injectors for the generation of a Taylor  $N_2$ -water flow and found  $\alpha_1 = 1.25$  and  $\alpha_2 = 2.27$  for the classical configuration where the gas is injected perpendicularly to the liquid flow with a gas injection channel width  $w_{in} = w$ .

Although the value of  $\alpha_2$  found in this study is consistent with what has been found by other studies, it is still slightly lower than what exists in the literature for rectangular channels. This relatively low value

of  $\alpha_2$  may indicate a lower leakage rate, which is coherent with the circular cross-section of the microchannel used. Indeed, less leakage flow may be expected for circular cross-sectional channels compared with rectangular cross-sectional channels, which is more prone leakage flow at the corners.

Völkel [31] proposed to use the same phenomenological model for bubble length to describe slug length:

$$\frac{L_S}{D_{in}} = \alpha_2 + \alpha_1 \frac{U_L}{U_G} \quad (13)$$

This model considers flat-ended bubbles and slugs and a negligible liquid film thickness. However, Fig. 7 shows that the coefficients  $\alpha_1$  and  $\alpha_2$  found for the slug length are different from those found for the bubble length. The same result has been found in the literature by Volkel [31], Abadie et al. [32] and Martin et al. [33] and is explained by the fact that the model does not take into account the volume of liquid around the heads and tails of the bubbles, nor in the film around the body of the gas bubble.

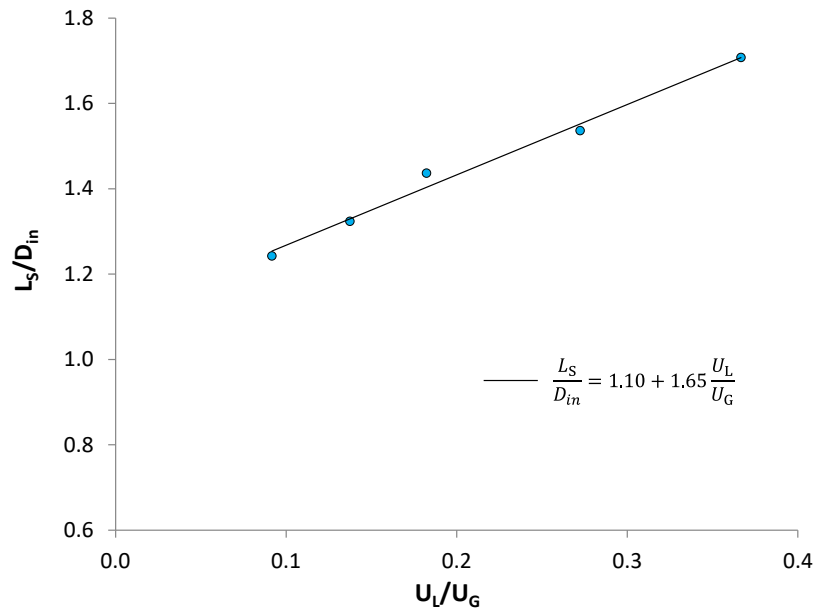


**Figure 7.** Variation of normalized slug length as a function of superficial velocity ratio ( $N_2$ -cyclohexane,  $T=40^\circ C$ ,  $P=20$  barg,  $3.4 < U_G < 13.7$  mm.s $^{-1}$ ,  $1.3 < U_L < 1.9$  mm.s $^{-1}$ ).

To directly link bubble and slug length to the operating conditions, Abadie [34] expressed the bubble length relative to the length of the unit cell as a function of the superficial velocities of each phase as follows:

$$\frac{L_B}{L_B + L_S} = \frac{U_G/U_L}{\beta + U_G/U_L} \quad (14)$$

with  $\beta$  a coefficient that takes into account the thickness of the liquid film around the body of the bubble and the liquid volume surrounding the bubble heads and tails.  $\beta = 1$  when the bubble caps are flat and there is no liquid film. Fig. 8 shows that by fitting the model in Equation (14) to the experimental data obtained in this study, a value of  $\beta = 0.84$  was found. This is the same as  $\beta = 0.83$  found by Martin et al. [33] for flow in a square cross-sectional microchannel and slightly higher than that found by Abadie [34] ( $\beta = 0.6$ ) for flow in a rectangular microchannel. The difference between the result found here and that of Abadie [34] is principally due to the range of operating conditions studied. In this study (and that of Martin et al. [33]), a small range of low capillary numbers ( $1.6 \cdot 10^{-2} < Ca < 4.5 \cdot 10^{-2}$ ) and low Reynolds numbers ( $29 < Re < 61$ ) were investigated that resulted in bubbles with near to hemispherical caps and negligible liquid film. Abadie [34] on the other hand applied the equation to points obtained over a significantly wider range of capillary numbers ( $6 \cdot 10^{-4} < Ca < 10^{-1}$ ) and Reynolds numbers ( $0.1 < Re < 231$ ). Such conditions result in a range of bubble shapes and film thickness (from symmetrical bubbles with hemispherical caps and negligible film thickness to bullet-shaped bubbles with significant film thickness) and therefore impact the value of  $\beta$ .

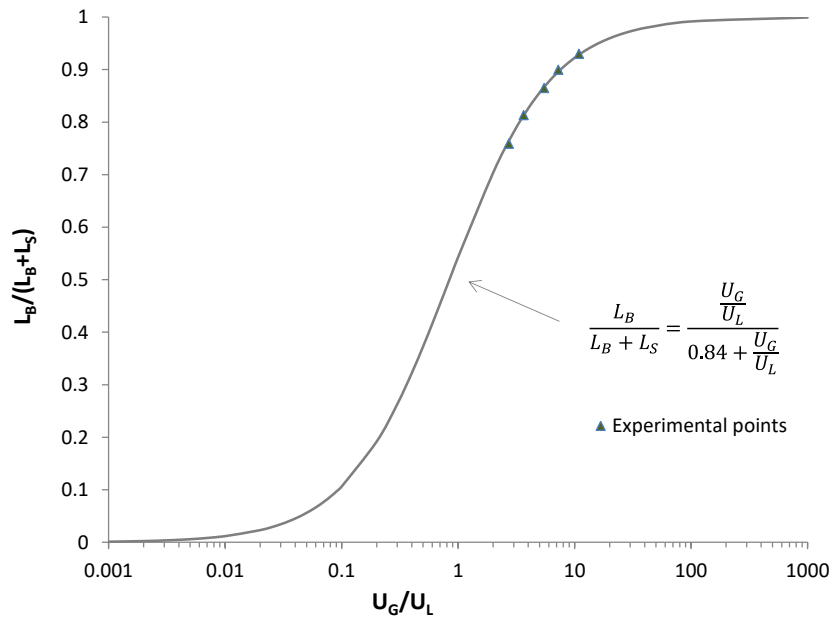


**Figure 8.** Variation of the bubble length to the unit cell length ratio as a function of the superficial velocity ratio ( $N_2$ -cyclohexane,  $T=40^\circ C$ ,  $P=20$  barg,  $3.4 < U_G < 13.7$  mm. $s^{-1}$ ,  $1.3 < U_L < 1.9$  mm. $s^{-1}$ )

### 3.1.2 Effect of lateral feed

The impact of the lateral feed on the stability of the Taylor flow was studied by performing tests at  $P=20$  barg and  $T=40^{\circ}\text{C}$  with a lateral feed of cyclohexane. The lateral feed is introduced at the second T-junction with two different flow rates  $Q_{L_2} = 0.1 \text{ mL}\cdot\text{h}^{-1}$  and  $0.2 \text{ mL}\cdot\text{h}^{-1}$ , which correspond to a liquid superficial velocities of  $U_{L_2} = 0.13 \text{ mm}\cdot\text{s}^{-1}$  and  $0.25 \text{ mm}\cdot\text{s}^{-1}$ , respectively. The ranges of gas and liquid flow rates in the main channel are same as in the previous part of this study.

Considering the low rates of the lateral feed, no impact on the bubble volume is expected. Indeed, Tab. 4 shows that the volume of the bubble and slug with and without lateral feed is approximately the same. Small variations can be noted in tests 2 and 4. These variations are of the order of  $\pm 6\%$ , which is much less than the coefficient of variation of the bubble volume that is about 8% for test 2 and 15% for test 4.

**Table 4.** Comparison of bubble and slug sizes with and without lateral feed ( $\text{N}_2$ -cyclohexane,  $T=40^{\circ}\text{C}$ ,  $P=20$  barg).

Test	$Q_G$ [ $\text{NmL}\cdot\text{h}^{-1}$ ]	$Q_L$ [ $\text{mL}\cdot\text{h}^{-1}$ ]	$Q_{L_2}$ [ $\text{mL}\cdot\text{h}^{-1}$ ]	$V_b$ [ $\text{mm}^3$ ]	$V_s$ [ $\text{mm}^3$ ]	Variation Coef. of $V_s$ [%]
1	50	1	0	0.50	0.19	4.24
			0.1	0.50	0.21	4.63
			0.2	0.50	0.22	4.77
2	100	1	0	0.88	0.17	4.50
			0.1	0.93	0.19	2.43
			0.2	0.88	0.20	1.86
3	100	1.5	0	0.63	0.18	2.51
			0.2	0.61	0.20	2.48
4	200	1	0	1.60	0.15	3.43
			0.2	1.69	0.18	2.60

Furthermore, the increase in capillary number due to the lateral feed is only between 2 and 5% of the value without the lateral feed. Therefore, using Equation (5), the increase in the thickness of the liquid film is only around 3%. Fig. 9 shows that the ratio of the slug volume with lateral feed to the slug volume without lateral feed is equal to the ratio of total liquid flow with lateral feed to liquid flow without

lateral feed to within  $\pm 5\%$ . This shows that after lateral injection, the added liquid volume is finally retained almost exclusively in the slug volume and is not held up in the liquid film.

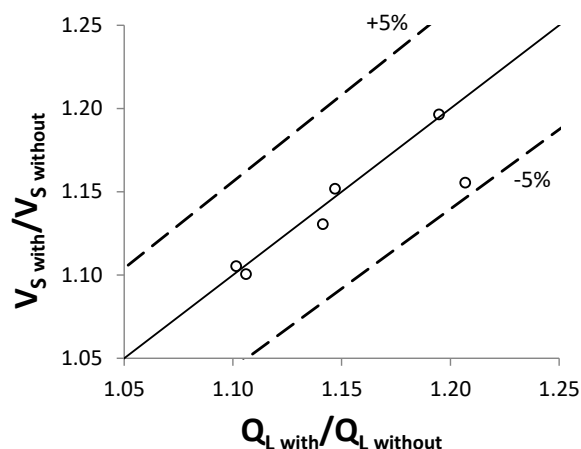


**Figure 9.** Increase of the slug volume according to the fraction of liquid added by lateral feed ( $N_2$ -cyclohexane,  $T=40^\circ C$ ,  $P=20$  barg)

Furthermore, it was found that the coefficient of variation for the slug volume under conditions with lateral feed compared with those without the lateral feed remains approximately the same or decreases, which means that the volume of liquid added to a slug by the lateral feed is the same for every slug. This result is important for the oligomerization reaction because it means that the amount of the catalyst in each liquid slug will be approximately the same along the microreactor and thus a homogeneous catalytic activity during an oligomerization test will be expected. Park et al. [4] tried to add their liquid phase catalyst to the Taylor flow by a lateral feed with the same configuration as proposed in this study. However, they found that the amount of the added liquid was not the same in each liquid slug as the Taylor flow was not sufficiently stable. As a solution, Park et al. [4] mixed the liquid catalyst with the liquid phase at low temperature in order to avoid side reactions and the gas phase was then dispersed in the liquid phase mixture. Premixing the catalyst with the liquid phase is not a viable solution in the current application since the contact of catalyst and activator in absence of ethylene can impact the catalytic performance.

Another important aspect that couldn't be addressed in this study is the mixing time of the catalyst in each liquid slug. Zaloha et al. [39] showed that in a Taylor flow a liquid element completes one

revolution in the liquid slug in the time required for the slug to travel approximately five times its own length, i.e.  $\sim 5L_S/U_{TP}$ . Thus, given that the average length of the slugs in this study is 0.6 mm, and the average  $U_{TP}$  is  $0.02 \text{ m}\cdot\text{s}^{-1}$  the liquid elements will need about 0.15 s to make a complete revolution. Even if several revolutions are needed to achieve complete mixing, and considering that the residence time of the liquid slug inside the reactor is usually greater than 60 s, it can be assumed that the catalyst mixing is a fast phenomenon compared to ethylene conversion.

### 3.1.3 Effect of pressure and temperature

In order to study the impact of pressure and temperature on bubble volume, Taylor flow was generated at two different operating pressures (10 and 27 barg) and two temperatures (30 and 50°C). The results were compared with those at 20 barg and 40°C.

Fig. 10a shows the variation in bubble generation frequency for three different pressures and two liquid flow rates. At a fixed liquid flow rate, the bubble generation frequency increases with an increase in the gas superficial velocity. By comparing the frequencies of bubble generation at equal superficial velocity ratios, Fig. 10a shows a slight increase in frequency with an increase in system pressure, which corresponds to a decrease in the bubble volume with pressure as shown in Fig. 10b. Indeed, an increase in operating pressure leads to a decrease of the surface tension and this in turn results in a decrease in interfacial stability, thereby facilitating the bubble pinch-off. Thus, it can be expected that shorter bubbles are generated since the bubble squeezing time is shorter. Yao et al. [35] however found an opposite trend and showed that the bubble formation period for a  $\text{N}_2$ -water dispersion was relatively longer at higher pressures. The authors explained this observation by the fact that the amount of leakage flow increases with pressure as they showed experimentally. Indeed, Yao et al. [35] used a rectangular cross-sectional channel where leakage can easily occur in the corners, however, for a circular cross-sectional channel as used in this study, a significantly lower amount of leakage flow may be expected thereby making the surface tension effect dominant. Nevertheless, the change in bubble volume with pressure is significantly small and therefore is considered negligible when estimating the bubble volume or length for an oligomerization reaction test.

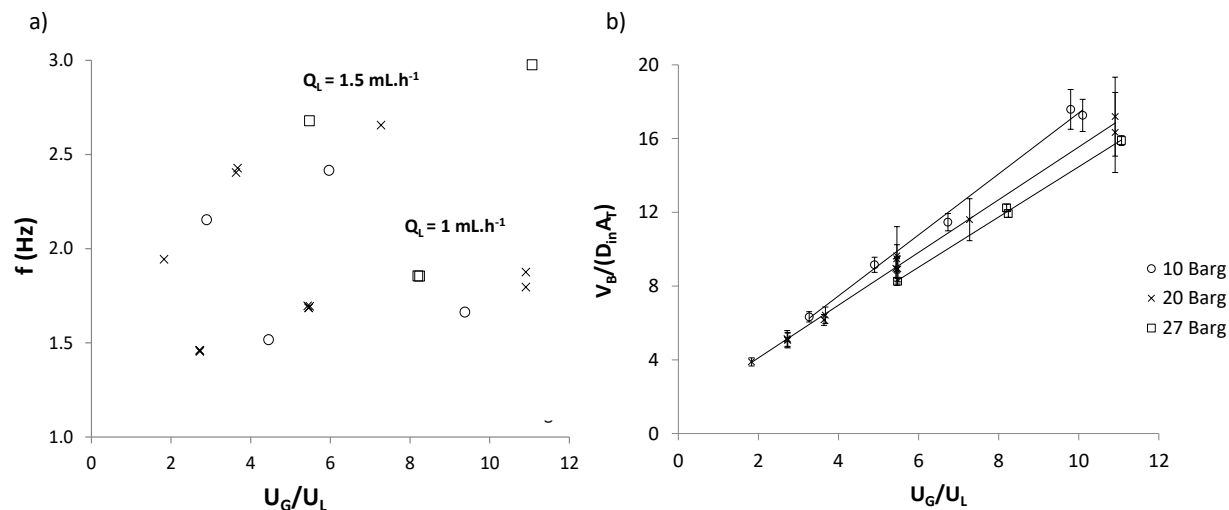


**Figure 10.** The effect of pressure on a) bubble formation frequency and b) normalized bubble volume, as a function of superficial velocity ratio ( $\text{N}_2$ -cyclohexane,  $T=40^\circ\text{C}$ ,  $3.4 < U_G < 20.9 \text{ mm.s}^{-1}$ ,  $1.3 < U_L < 1.9 \text{ mm.s}^{-1}$ )

The variation of the bubble volume as a function of the superficial velocity ratio for three different temperatures was also studied. The influence of temperature on the bubble volume was found to be negligible even if the surface tension decreases slightly with an increase in temperature. Indeed, an increase in the temperature also decreases the viscosity of the continuous phase, and thus decreases the shear stress exerted on the gas tip, which may counterbalance the effect of a decrease in surface tension.

### 3.2 Mass transfer

A segmented flow of ethylene and cyclohexane was generated in order to evaluate the mass transfer performance of the system. The mass transfer of ethylene to the liquid phase was evaluated by tracking the bubble volume along the capillary channel and the mass transfer coefficient was estimated based on the decrease in bubble volume. The gas and the liquid phase flow rates were varied in the range ( $50 < Q_G < 370 \text{ NmL.h}^{-1}$ ,  $0.5 < Q_L < 4 \text{ mL.h}^{-1}$ ) for three operating pressures (10, 20 and 27 barg) and two temperatures (30 and  $40^\circ\text{C}$ ).

The first step of the study was to verify the decrease in bubble size that captures the transfer of ethylene into the liquid phase. By tracking bubbles at the first position in the acquisition window ( $z/D=53$  in Fig. 5), two types of observations were made depending on the operating conditions:

- For conditions with relatively low gas and liquid superficial velocities, a constant bubble volume was observed at the first position in the acquisition window or just a few millimeters after this position.
- For conditions with relatively high gas and liquid superficial velocities, the bubble volume decreases from  $z/D=53$  and then tends to a constant value.

For the other two positions ( $z/D=1250$  and  $z/D=2500$ ), no change in bubble volume was detected.

Therefore, for the range of operating conditions explored, mass transfer took place between the generation point of Taylor flow in the T-junction and the end of capillary noted as *Line 1* in the acquisition window in Fig. 5. The gas-liquid dispersion then reaches thermodynamic equilibrium, which is indicated by a constant bubble size. For the conditions where no significant decrease in the bubble volume was detected, it was not possible to determine a  $K_L a$ . The only conditions for which a significant decrease in the bubble volume was detected are experiments at 40°C and a pressure of 20 barg or 27 barg. Thus, the interpretation of the  $K_L a$  results was done independently of the pressure effects.

The volumetric mass transfer coefficient was calculated by using the measured bubble volumes in Equation (12).  $V_B^i$  is defined as the volume of the first bubble detected in the acquisition window,  $z_i$  is the position of this bubble and the equilibrium bubble volume  $V_B^{eq}$  is the bubble volume at the reactor outlet. Fig. 11b shows the variation of  $K_L a$  as a function of the two-phase superficial velocity. This figure shows an increase in the volumetric mass transfer coefficient with an increase in the total flow rate in the reactor. Indeed, in Taylor flow, the increase in two phase flow velocity results in increased recirculation in the liquid slug, thus enhancing  $K_L$ . Fig. 11a shows that for a fixed flow rates ratio  $Q_L/Q_G$  the  $K_L a$  coefficient increases with an increase of  $Q_G$  as the flow velocity will increase with a specific surface that remains almost constant. Fig. 11a also shows that for a fixed gas flow rate,  $K_L a$  increases with an increase of the ratio  $Q_L/Q_G$ , despite the fact that the increase of this ratio leads to the decrease

of the bubble length and the decrease of the specific surface  $a$ . These results indicate that the effect of the increase in flow rate on mass transfer may be dominant in this study.

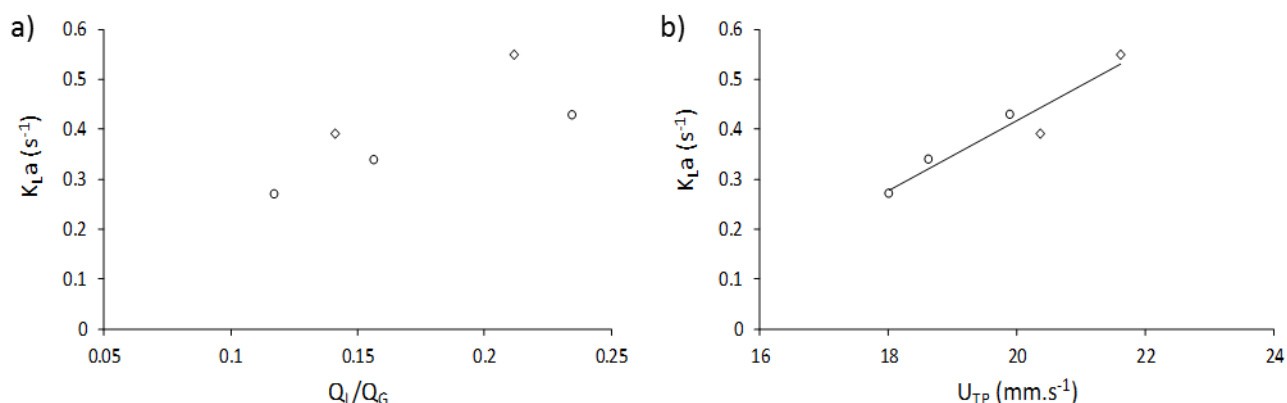


**Figure 11.** Variation of the global volumetric mass transfer coefficient in function of a) the flow rate ratio, b) the two-phase superficial velocity (○:  $Q_G=12.80 \text{ mL}\cdot\text{h}^{-1}$ ; ◇:  $Q_G=14.17 \text{ mL}\cdot\text{h}^{-1}$ )

The experimental  $K_L a$  values obtained in this study were compared with those obtained with the equation proposed by Vandu et al. [14]. This equation was chosen as it was validated with experiments carried out in a geometry close to that used in this study (circular tube with 1 mm inner diameter) and for low capillary numbers ( $Ca < 10^{-2}$ ). The values obtained with Vandu et al.'s [14] equation are between  $0.6 \text{ s}^{-1}$  and  $0.9 \text{ s}^{-1}$  for the selected operating conditions; these predicted values are slightly greater than the experimental values found here. This difference can be due to the fact that the  $K_L a$  obtained experimentally were not calculated directly between the microchannel inlet, where the gas and liquid are contacted, and thermodynamic equilibrium but after bubble generation. Indeed, Deleau et al. [20] showed that the volumetric mass transfer coefficient of  $\text{CO}_2$  in water was not the same along the length of the capillary tube and that it was notably greater in the bubble generation zone. They showed that about 20% of the equilibrium concentration was reached during the bubble generation process. It may therefore be considered that lower experimental values found here are due to the fact that mass transfer directly in the bubble generation zone was not accounted for.

In order to compare the mass transfer rate with the reaction kinetics, the Hatta number was calculated considering a catalyst concentration of 31 ppm and a reaction rate constant based on stirred tank reactor experiments. In these conditions, the Hatta number varies between 0.13 and 0.50, indicating

that the mass transfer rate in the liquid film is faster than the reaction kinetics. This result also shows that the flow rate range represents the lower limit of the operating conditions that can be used to perform the ethylene oligomerization reaction without mass transfer limitation.

### 3.3 Oligomerization reaction

In order to validate the proof-of-concept of the use of a microchannel reactor for oligomerization catalyst screening, an ethylene oligomerization test was performed in the microreactor unit. Special care was taken to ensure the elimination of humidity and impurities.

Tab. 5 shows the principle results of the oligomerization reaction test performed in the microreactor unit. The injection flowrates resulted in a catalyst concentration of 31.4 ppm in the liquid slugs at the reactor inlet. For a residence time of 1.1 minutes, the microreactor yielded a 29.7% ethylene conversion. This moderate conversion level enabled segmented gas-liquid flow to be maintained along the entire length of the microreactor, and was high enough to measure butene, 1-butene, hexane and octane selectivities.

This first attempt showed that the developed microreactor unit can be used to perform ethylene oligomerization reactions in the defined conditions. Compared to screening oligomerization catalysts in fed-batch stirred tank reactors, the microreactor offers low residence time and a continuous operation that allow testing several operating conditions in a shortened time. However, more experiments are required in order to develop a well-defined protocol for the screening of the ethylene oligomerization catalysts using the microreactor unit.

**Table 5.** Performance of the oligomerization reaction carried out in the microreactor unit.

Temperature (°C)	45
Pressure (bar)	20
C <sub>2</sub> H <sub>4</sub> flow rate (NmL.h <sup>-1</sup> )	286
Catalyst solution flow rate (mL.h <sup>-1</sup> )	0.18
Activator solution flow rate (mL.h <sup>-1</sup> )	0.11
Solvent flow rate (mL.h <sup>-1</sup> )	1.00
Residence time (min)	1.1
Conversion C <sub>2</sub> H <sub>4</sub> (% weight)	29.7
Butene selectivity C4 (wt. %)	86.1
1-butene/butene selectivity (wt. %)	73.3
Hexene selectivity (wt. %)	12.4

#### 4 Conclusion

In order to develop a microreactor unit for catalytic screening tests for oligomerization reactions, a hydrodynamic and mass transfer study was carried in order to characterize the gas-liquid Taylor flow and evaluate mass transfer capacity of the microreactor. An oligomerization reaction was then performed in the microreactor unit in order to validate its proof-of-concept.

The hydrodynamics in a non-reactive system with no mass transfer was studied with N<sub>2</sub>-cyclohexane flow performed under different operating conditions (including varying flow rates, pressure and temperature). Bubble and slug length vary linearly with the superficial velocity ratio, following the Garstecki et al. model [3] and in agreement with the results of similar studies in the literature. The bubble and slug length equations identified for the operating conditions of the oligomerization reaction provide knowledge on which flow rates must be used for catalytic reaction screening such that Taylor flow is maintained along the length of microreactor. A slight effect of pressure on the bubble volume was observed: for a fixed superficial velocities ratio, the bubble volume decreases about 5% of its initial value with an increase in pressure of 10 bar. There was found to be no significant effect of temperature on the bubble volume. In conclusion, the impact of both pressure and temperature on the bubble volume in the range of the study was not sufficiently significant to be considered in the estimation of the bubble length.

The impact of a lateral feed on Taylor flow was explored in order to mimic the catalyst feed in an oligomerization reaction. The experiments showed that the liquid slug volume increases proportionally to the additional flow rate. This suggests that the majority of the liquid in the lateral feed is ultimately retained in the liquid slug rather than in the liquid film around the bubble body. As a result, it can be expected that in the case of a catalyst feed, the concentration of the catalyst in each slug will be approximately the same for every slug, which is primordial for performing catalytic test reactions.

A series of ethylene-cyclohexane flow experiments were performed in the range of operating conditions for the oligomerization reaction in order to verify that the catalytic tests can be conducted without being limited by mass transfer. The results show that the values of the volumetric mass transfer coefficients in the range of conditions studied are between  $0.27 \text{ s}^{-1}$  and  $0.55 \text{ s}^{-1}$ . These values lead to a Hatta number between 0.13 and 0.50 for ethylene oligomerization reaction. It can therefore be considered that the ethylene oligomerization reaction in the microreactor and in the defined conditions will not be limited by mass transfer.

Finally, the ethylene oligomerization reaction was performed using the new microreactor unit in order to validate the proof-of-concept of the continuous microreactor system. The test showed that the microreactor was able to perform ethylene oligomerization reaction in the defined conditions, thus allowing measuring the performances of the catalytic system faster than fed-batch stirred tank reactors and with a better thermal control. Nevertheless, more experiments under different operating conditions are still required in order to further evaluate the performance of the microreactor itself, and to define a protocol for the screening of the ethylene oligomerization catalysts.

### Formatting of funding sources

This research did not receive any specific grant from funding agencies in the public, commercial, or not-for-profit sectors.

### Symbols used

$a$	$[\text{m}^{-1}]$	Gas-liquid specific surface area
$A_T$	$[\text{m}^2]$	T-junction cross-sectional area
$Ca$	$[-]$	Capillary number based on two phases superficial velocity
$C$	$[\text{mol} \cdot \text{m}^{-3}]$	Concentration
$C_p$	$[\text{J} \cdot \text{kg}^{-1} \cdot \text{K}^{-1}]$	Heat capacity
$d$	$[\text{m}]$	Characteristic width of the bubble neck
$D$	$[\text{m}]$	Internal diameter
$D_{in}$	$[\text{m}]$	Dispersed phase inlet diameter
$D_{ch}$	$[\text{m}]$	Main channel internal diameter
$D_{iff}$	$[\text{m}^2 \cdot \text{s}^{-1}]$	Gas diffusion rate
$K_L$	$[\text{m} \cdot \text{s}^{-1}]$	Overall liquid side mass transfer coefficient

$L$	[m]	Length
$P$	[bar]	Pressure
$Q$	[mL.h <sup>-1</sup> ]	Flow rate
$R$	[m]	Channel radius
$Re$	[-]	Reynolds number
$t$	[s]	Time
$T$	[°C]	Temperature
$U$	[m.s <sup>-1</sup> ]	Velocity
$v$	[m <sup>3</sup> .mol <sup>-1</sup> ]	Molar volume
$V$	[m <sup>3</sup> ]	Volume
$w$	[m]	Continuous phase inlet width
$w_{in}$	[m]	Dispersed phase inlet width
$z$	[m]	Axial position in the channel

#### Greek letters

$\alpha, \alpha_1, \alpha_2, \beta$	[-]	Constants
$\delta$	[m]	Liquid film thickness
$\mu$	[mPa.s]	Dynamic Viscosity
$\rho$	[kg.m <sup>-3</sup> ]	Density
$\sigma$	[N.m <sup>-1</sup> ]	Surface tension

#### Sub- and Superscripts

$B$	Bubble
$C$	Critical
$eq$	At equilibrium
$G$	Gas
$i$	Initial
$L$	Liquid
$S$	Slug
$TP$	Two phase

#### References

- [1] P.-A. R. Breuil, L. Magna, H. Olivier-Bourbigou, *Catal Lett* **2015**, *145* (1), 173–192. DOI: 10.1007/s10562-014-1451-x.
- [2] D. S. McGuinness, *Chemical reviews* **2011**, *111* (3), 2321–2341. DOI: 10.1021/cr100217q.
- [3] A. Forestière, H. Olivier-Bourbigou, L. Saussine, *Oil & Gas Science and Technology - Rev. IFP* **2009**, *64* (6), 649–667. DOI: 10.2516/ogst/2009027.

- [4] C. P. Park, M. M. van Wingerden, S.-Y. Han, D.-P. Kim, R. H. Grubbs, *Organic letters* **2011**, *13* (9), 2398–2401. DOI: 10.1021/ol200634y.
- [5] J. Keybl, K. F. Jensen, *Ind. Eng. Chem. Res.* **2011**, *50* (19), 11013–11022. DOI: 10.1021/ie200936b.
- [6] C. de Bellefon, S. Caravieilhés, P. Grenouillet, in *Microreaction Technology* (Eds: M. Matlosz, W. Ehrfeld, J. P. Baselt), Springer Berlin Heidelberg, Berlin, Heidelberg **2001**, 408–413.
- [7] C. de Bellefon, R. Abdallah, T. Lamouille, N. Pestre, S. Caravieilhés, P. Grenouillet, *Chimia* **2002**, *56* (11), 621–626. DOI: 10.2533/000942902777680018.
- [8] J. S. Moore, K. F. Jensen, *Angew. Chem.* **2014**, *126* (2), 480–483. DOI: 10.1002/ange.201306468.
- [9] L. Vanoye, M. Pablos, C. de Bellefon, A. Favre-Réguillon, *Adv. Synth. Catal.* **2015**, *357* (4), 739–746. DOI: 10.1002/adsc.201400925.
- [10] L. Vanoye, M. Pablos, N. Smith, C. de Bellefon, A. Favre-Réguillon, *RSC Adv* **2014**, *4* (100), 57159–57163. DOI: 10.1039/c4ra12067a.
- [11] S. Haase, D. Y. Murzin, T. Salmi, *Chemical Engineering Research and Design* **2016**, *113*, 304–329. DOI: 10.1016/j.cherd.2016.06.017.
- [12] S. Irandoust, S. Ertlé, B. Andersson, *Can. J. Chem. Eng.* **1992**, *70* (1), 115–119. DOI: 10.1002/cjce.5450700116.
- [13] G. Berc̃ic̃, A. Pintar, *Chemical Engineering Science* **1997**, *52* (21-22), 3709–3719. DOI: 10.1016/S0009-2509(97)00217-0.
- [14] C. O. Vandu, H. Liu, R. Krishna, *Chemical Engineering Science* **2005**, *60* (22), 6430–6437. DOI: 10.1016/j.ces.2005.01.037.
- [15] J. Yue, G. Chen, Q. Yuan, L. Luo, Y. Gonthier, *Chemical Engineering Science* **2007**, *62* (7), 2096–2108. DOI: 10.1016/j.ces.2006.12.057.
- [16] J. Yue, L. Luo, Y. Gonthier, G. Chen, Q. Yuan, *11th International Conference on Gas-Liquid and Gas-Liquid-Solid Reactor Engineering* **2009**, *64* (16), 3697–3708. DOI: 10.1016/j.ces.2009.05.026.
- [17] S. Kuhn, K. F. Jensen, *Ind. Eng. Chem. Res.* **2012**, *51* (26), 8999–9006. DOI: 10.1021/ie300978n.
- [18] N. Dietrich, K. Loubière, M. Jimenez, G. Hébrard, C. Gourdon, *11th International Conference on Gas-Liquid and Gas-Liquid-Solid Reactor Engineering* **2013**, *100* (Supplement C), 172–182. DOI: 10.1016/j.ces.2013.03.041.
- [19] C. Yao, Z. Dong, Y. Zhao, G. Chen, *Chemical Engineering Science* **2014**, *112* (Supplement C), 15–24. DOI: 10.1016/j.ces.2014.03.016.
- [20] T. Deleau, M.H.H. Fechter, J.-J. Letourneau, S. Camy, J. Aubin, A. S. Braeuer, F. Espitalier, *11th International Conference on Gas-Liquid and Gas-Liquid-Solid Reactor Engineering* **2020**, *228*, 115960. DOI: 10.1016/j.ces.2020.115960.
- [21] P. Garstecki, M. J. Fuerstman, H. A. Stone, G. M. Whitesides, *Lab on a chip* **2006**, *6* (3), 437–446. DOI: 10.1039/b510841a.
- [22] V. van Steijn, M. T. Kreutzer, C. R. Kleijn, *Chemical Engineering Science* **2007**, *62* (24), 7505–7514. DOI: 10.1016/j.ces.2007.08.068.
- [23] M. Abolhasani, M. Singh, E. Kumacheva, A. Günther, *Lab on a chip* **2012**, *12* (9), 1611–1618. DOI: 10.1039/c2lc21043f.
- [24] J. Tan, Y. C. Lu, J. H. Xu, G. S. Luo, *Chemical Engineering Journal* **2012**, *185-186*, 314–320. DOI: 10.1016/j.cej.2012.01.054.

- [25] W. Li, K. Liu, R. Simms, J. Greener, D. Jagadeesan, S. Pinto, A. Günther, E. Kumacheva, *Journal of the American Chemical Society* **2012**, *134* (6), 3127–3132. DOI: 10.1021/ja2101278.
- [26] M. Sattari-Najafabadi, M. Nasr Esfahany, Z. Wu, B. Sunden, *Chemical Engineering and Processing - Process Intensification* **2018**, *127*, 213–237. DOI: 10.1016/j.cep.2018.03.012.
- [27] P. Sobieszuk, J. Aubin, R. Pohorecki, *Chem. Eng. Technol.* **2012**, *35* (8), 1346–1358. DOI: 10.1002/ceat.201100643.
- [28] J. M. van Baten, R. Krishna, *Chemical Engineering Science* **2004**, *59* (12), 2535–2545. DOI: 10.1016/j.ces.2004.03.010.
- [29] J.-N. Jaubert, F. Mutelet, *Fluid Phase Equilibria* **2004**, *224* (2), 285–304. DOI: 10.1016/j.fluid.2004.06.059.
- [30] A. Leclerc, R. Philippe, V. Houzelot, D. Schweich, C. de Bellefon, *Chemical Engineering Journal* **2010**, *165* (1), 290–300. DOI: 10.1016/j.cej.2010.08.021.
- [31] N. Völkel, *Design and characterization of gas-liquid microreactors*, Ph.D Thesis, INP Toulouse, Toulouse France **2009**.
- [32] T. Abadie, J. Aubin, D. Legendre, C. Xuereb, *Microfluid Nanofluid* **2012**, *12* (1-4), 355–369. DOI: 10.1007/s10404-011-0880-8.
- [33] A. Martin, S. Camy, J. Aubin, *11th International Conference on Gas-Liquid and Gas-Liquid-Solid Reactor Engineering* **2018**, *178*, 297–311. DOI: 10.1016/j.ces.2017.12.046.
- [34] T. Abadie, *Hydrodynamics of gas-liquid taylor flow in microchannels*, Ph.D Thesis, INP Toulouse, Toulouse France **2013**.
- [35] C. Yao, Z. Dong, Y. Zhao, G. Chen, *AIChE J.* **2014**, *60* (3), 1132–1142. DOI: 10.1002/aic.14306.
- [36] R. Pohorecki, *Chemical Engineering Science* **2007**, *62* (22), 6495–6498. DOI: 10.1016/j.ces.2007.07.015.
- [37] T. Nitta, A. Tatsuishi, T. Katayama, *Journal Of Chemical Engineering Of Japan* **1974**, *6* (6), 475–480. DOI: 10.1252/jcej.6.475.
- [38] J.J. Jasper, *Journal of Physical and Chemical Reference Data 1* **1972**, 841–1010. DOI: 10.1063/1.3253106
- [39] P. Zaloha, J. Kristal, V. Jiricny, N. Völkel, C. Xuereb, J. Aubin, *Chemical Engineering Science* **2012**, *68* (1), 640–649. DOI: 10.1016/j.ces.2011.10.036.